Local dynamics and structure of pure and Ta substituted $(K_{1-x}Na_x)NbO_3$ from first principles calculations

Malliga Suewattana
Department of Physics, Faculty of Science, Mahidol University, Bangkok 10400, Thailand

David J. Singh
Material Science and Technology Division, Oak Ridge National Laboratory, Oak Ridge, Tennessee 37831-6114, USA

(Received 20 April 2010; revised manuscript received 11 July 2010; published 28 July 2010)

The local structure and dynamics of piezoelectric $K_{1-x}Na_xNbO_3$ perovskite solid solutions with and without partial Ta substitution at $x=0.5$ are investigated using first principles calculations for supercells. The results are analyzed locally using the dynamical pair distribution functions. The local structures for Ta-substituted material show smaller off-centering of Ta compared to Nb. In addition, the dynamics of the relaxed structure indicate softer Nb force constants relative to Ta even though the Nb has shorter O nearest-neighbor distances than Ta. These results are discussed in relation to experimental measurements which show a decrease in Curie temperature and an increase in dielectric constant when Ta is partially substituted into $K_{1-x}Na_xNbO_3$.

DOI: 10.1103/PhysRevB.82.014114 PACS number(s): 77.84.Bw, 77.84.Ek

I. INTRODUCTION

There has been renewed interest in non-Pb-based ferroelectrics and piezoelectrics both because of technological interest in so-called green materials and because of the different characteristics that some of these materials have, e.g., the high Curie temperatures, T_C, of some $(K,Na)NbO_3$-based compositions and the large polarizations in some Bi-based ferroelectrics, e.g., $BiFeO_3$. Textured material based on $(K,Na)NbO_3$ (KNN) can exhibit good piezoelectric properties and are comparable to $Pb(Zr,Ti)P_3$ (PZT) ceramics. This was demonstrated by Saito and co-workers using a KNN-based material with addition of Li, Ta, and Sb.[1] The dielectric and piezoelectric properties as well as the structure and phase diagram have been the subjects of recent experimental and theoretical investigations.[2–11] $AgNbO_3$ has also been shown to be an interesting ferroelectric with large polarization.[12,13] However, in comparison with the extensively studied PZT materials, KNN-based piezoelectrics appear to be more complicated especially from the point of view of the rather complex composition temperature phase diagrams.[14–17] KNN shows a morphotropic phase boundary at around 50% K and 50% Na separating orthorhombic and tetragonal phase.[3,6,18,19] Although this is different from PZT where the morphotropic phase boundary (MPB) is between tetragonal and rhombohedral phases, an enhancement in response related properties at compositions close to the MPB is found, as in PZT. Nonetheless, the electromechanical properties of KNN are generally inferior to those of PZT.

As mentioned, various substitutions on the perovskite *A* site and *B* site have been investigated to enhance the ferroelectric and piezoelectic performance of KNN. These include studies of $(Na,K,Li)NbO_3$ ternary system and the addition of Sb, Ta, or Cu on the *B* sites.[3,20–29] Also, the extreme case of substituting high concentrations of Li into $KNbO_3$ was investigated using first principles calculations and shown to be an interesting ferroelectric if it can be made in perovskite form.[30] Among those, it is known that Ta substitution of Nb changes the properties of $KNbO_3$ and, in particular, small amounts of Ta substitution for Nb can enhance the piezoelectric properties of KNN ceramics while reducing the T_C.[31] While structural differences in oxides can often be understood in terms of steric considerations, particularly using ionic radii, the ionic radii of octahedral Ta^{5+} and Nb^{+5} are practically identical.[32] Nonetheless, the ferroelectric distortions of niobates and tantalates are quite distinct. For example, $KNbO_3$ is a well-known ferroelectric with a rhombohedral ground state but $KTaO_3$ remains cubic down to the lowest temperatures. The difference is due to the different chemistry of Ta and Nb, which leads to less O *p*-*B*-site *d* hybridization in the tantalate. This, combined with the fact that this type of hybridization favors ferroelectricity,[33] is sufficient to explain the different structures of $KNbO_3$ and $KTaO_3$.[34]

Both ionic size and covalency represent short-range phenomena. In addition, long-range Coulomb interactions play a critical role in ferroelectricity. These different interactions make the question of the local structure nontrivial in solid solutions such as KNN with partial Ta substitution (denoted KNNT in the following). For example, do the *B*-site ions off-center in a cooperative way with little difference in the local Ta and Nb environments or is the Ta significantly less off-centered than the Nb reflecting its different chemistry? Turning to the dynamics, the force constants relevant to the ferroelectric mode are softer $KNbO_3$ than in $KTaO_3$ in the cubic phase but then stiffen below T_C so that at low-temperature $KTaO_3$ has softer behavior. This is because the Nb in $KNbO_3$ has shorter nearest O distances than the Ta in $KTaO_3$. Does this behavior carry over into KNNT so that the Ta force constants are essentially softer than those of Nb in the ferroelectric phase, or conversely are the force constants stiffer reflecting the less covalent chemistry of Ta, or perhaps some feature of the local structures?

Light can be shed on these and related questions by studying local structures using diffuse scattering to determine pair distribution functions (PDFs),[35–37] and with new techniques on inelastic scattering that yields local dynamical information, such as dynamical pair distribution function.[37] Compli-

mentary to this is the use of first principles calculations in supercells, which provide local structural and dynamical information directly, through approximations in the treatment of the alloy order, temperature effects and also in the solution of the electronic problems within density-functional theory. Here we apply this approach to KNN and KNNT at the harmonic level to obtain information about the local behavior of Ta relative to that of Nb in KNN-based material. We use PDF analysis. This is useful for understanding local structures in the presence of disorder, and which also may be convenient for comparison with experiments.

II. FIRST PRINCIPLES METHOD AND SUPERCELLS

The first principles calculations reported here were done within the local-density approximation using the general potential linearized augmented plane-wave (LAPW) method.[38] Local-orbital extensions[39] were used to treat the cation semicore states and to relax linearization errors.[40] Well-converged basis sets consisting of approximately 2500 LAPW functions for 20-atom supercells were used with LAPW sphere radii R_{MT} of $2.0a_0$ and $1.53a_0$ for the cations and oxygen, respectively. This corresponds to Ta basis-set cutoff, $k_{\max}$ of $7.0/R_{MT}$ for oxygen. The Brillouin-zone samplings were done with $4\times4\times4$ special k-point meshes. The results are based on supercell calculations for 20-atom cells of compositions $(K_2Na_2)Nb_4O_{12}$ and $(K_2Na_2)(Nb_3Ta)O_{12}$ using the experimental perovskite lattice parameter of 3.982 Å. These cells were constructed by adopting bcc-like lattice vectors $(-a,a,a)$, $(a,-a,a)$, and $(a,a,-a)$ but with no symmetry imposed. In order to investigate the dynamics, we first fully relaxed the internal coordinates of the atoms in each supercell. For both the pure and Ta-substituted cases, the structures were found to be ferroelectric with off-centering of Na and the B-site cations with respect to their O cages (the local structures obtained are described below in terms of their PDF). We then used a direct frozen phonon method to calculate the vibrational frequencies and eigenvectors for the supercells. This was done by imposing small displacements for each atom along each of the three Cartesian directions and calculating the resulting forces. The dynamical matrix was then constructed. For the low-frequency modes, additional calculations were done with displacement patterns corresponding to the eigenvectors. This was added to the data set to improve the accuracy, and the dynamical matrix was refit to obtain the final frequencies and normal modes.

This allows us to obtain the PDF as a function of temperature in the harmonic approximation. The PDF is defined as

$$\rho_{ij}(r) = \frac{1}{2\pi}\int dq e^{-iqr}\langle e^{iqr_{ij}}\rangle, \tag{1}$$

where q refers to the wave vector and r_{ij} is the distance between atom i and atom j. In a perfect classical crystal at 0 K, this would be a sum of Kronecker delta functions δ_{ij} at the r_{ij} interatomic distance. In a real system, atoms vibrate about the equilibrium due to the thermal and zero-point motion. The PDF, hence, is represented by the Gaussian broadening with the peaks at r_{ij}. We incorporate the dynamics of the harmonic and thermal motion into the PDF by applying the Debye-Waller approach.[41–43] In the harmonic approximation, the interatomic distance is denoted as $r_{ij}=r_{ij}^0+\mathbf{u}_{ij}\cdot\hat{r}_{ij}$. This yields

$$\langle e^{iqr_{ij}}\rangle = e^{iqr_{ij}^0}e^{-(1/2)q^2\langle(\mathbf{u}_{ij}\cdot\hat{r}_{ij})\rangle}. \tag{2}$$

By mean of the Debye-Waller theorem, the PDF ρ_{ij} is rewritten as

$$\rho_{ij}(r) = \frac{1}{2\pi}\int_{-\infty}^{\infty} e^{-(1/2)q^2\langle[\mathbf{u}_{ij}\cdot\hat{r}_{ij}]^2\rangle+iq(r_{ij}^0-r)}dq$$

$$= \frac{1}{\sqrt{2\pi\langle[\mathbf{u}_{ij}\cdot\hat{r}_{ij}]\rangle}}e^{-(r_{ij}^0-r)/2\langle[\mathbf{u}\cdot\hat{r}_{ij}]^2\rangle}. \tag{3}$$

Here the PDF is the Gaussian function with the peaks at r_{ij} and undergo the thermal broadening with the factor $\sigma_{ij}=\langle[\mathbf{u}_{ij}\cdot\hat{r}_{ij}]\rangle^{1/2}$. In the harmonic approximation and the system of N, one can express σ_{ij} as

$$\sigma_{ij}^2 = \frac{2\hbar}{N}\sum_{\mathbf{k},s}\frac{1}{\omega_s^2(\mathbf{k})}\left(\langle n_{k,s}\rangle+\frac{1}{2}\right)\left(\frac{1}{2}\left\{\frac{|e_i(\mathbf{k},s)\cdot\hat{r}_{ij}|}{M_i}+\frac{|e_j(\mathbf{k},s)\cdot\hat{r}_{ij}|}{M_j}\right\}-\frac{|e_i(\mathbf{k},s)\cdot\hat{r}_{ij}||e_j(-\mathbf{k},s)\cdot\hat{r}_{ij}|e^{i\mathbf{k}\cdot r_{ij}}}{\sqrt{M_iM_j}}\right), \tag{4}$$

where the wave vector $\mathbf{k}$ runs from 1 to $\mathcal{N}$, the branch number s runs from 1 to 3, ω_s is the frequency of the vibrating modes, and $e_i(\mathbf{k},s)$ are eigenvectors of dynamical matrix associated with branch s and projecting onto atom i.[43,44] The M_i are the atomic masses and the $\langle n_{k,s}\rangle$ is the occupation number following Bose-Einstein statistics. The dynamical PDF can be obtained in the same way after binning the normal modes into frequency ranges.

We emphasize that this harmonic level treatment provides information only about the dynamics of the low-temperature structure. It does not include anharmonic phonon coupling and therefore cannot describe the transition to the high-temperature nonferroelectric phase. While temperature dependence is shown to better elucidate the dynamics and to allow extracting of the anharmonic contribution by comparison with experiment when data become available, it should be born in mind that the present results are only physical for the dynamics of the low-temperature structure.

III. RESULTS AND DISCUSSION

As mentioned, the results are an analysis of the structure and harmonic vibrations of KNN and KNNT supercells. Figure 1 gives the calculated vibrational density of states, determined from the zone-center modes of the supercells with a broadening. The profiles of the density of states are similar for both cases in the high-frequency region showing similar O dynamics. It is to note the distinct peak at around 875 cm^{-1} in KNN and 880 cm^{-1} in KNNT which consisting of three phonon modes. These come from the symmetric O breathing modes. There are three such optic modes allowed

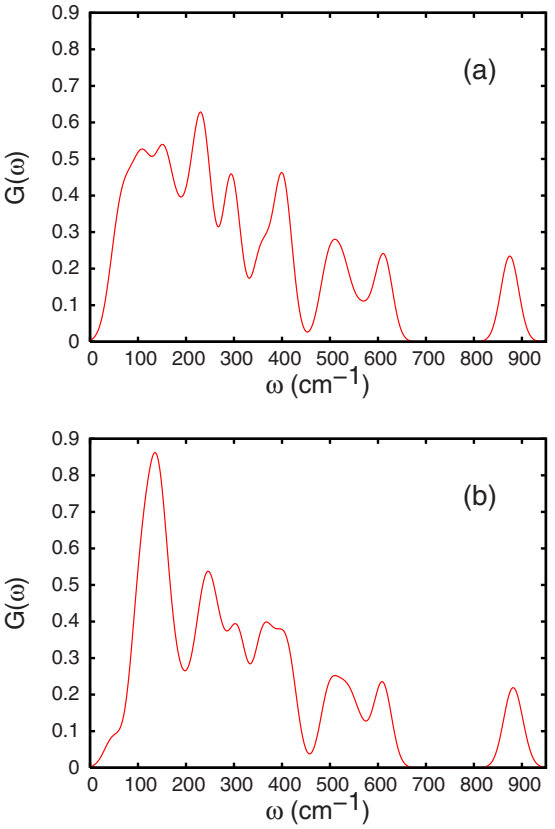

FIG. 1. (Color online) Calculated vibrational density of states for (a) KNN supercell and (b) KNNT supercell.

in a four perovskite unit supercell since the fully in-phase combination is not allowed. The lower frequency region shows more differences, which may be related both to force constant changes and the higher mass of Ta.

We begin by giving the main results for the PDF of the KNN and KNNT supercells. In order to better understand the local structure and dynamics, we decompose these into atomic contributions. We note that in Eq. (3), we sum only over the zone-center ($k=0$) modes in the reciprocal space. The large supercell in real space implies that the sum over first Brillouin zone is well resolved by summing only at the Γ point. Figure 2 shows the partial PDF of the *B*-site cations. This is defined as the part of the PDF that comes form only those pairs where the first atom in the pair is the *B*-site ion in question. The peak positions show the local structure while the broadening temperature provides information about the local dynamics. At high temperature, where the Dulong-Petit law holds, the mean-square displacements directly reflect force constants. The same is true for the dynamical PDF. Thus a rapid broadening of a PDF peak with temperature would indicate that phonons with eigenvectors that change the corresponding interatomic distance have soft effective force constants while a peak that stays sharp as temperature increases would show stiff force constants connecting atoms at that corresponding distance.

As may be seen (Fig. 2), there are significant differences between Nb and Ta local structures in KNNT. The first peak (in the ideal cubic structure at 1.99 Å) corresponds to the O cage of the *B* site. The structures at ≈3.45 Å, and at

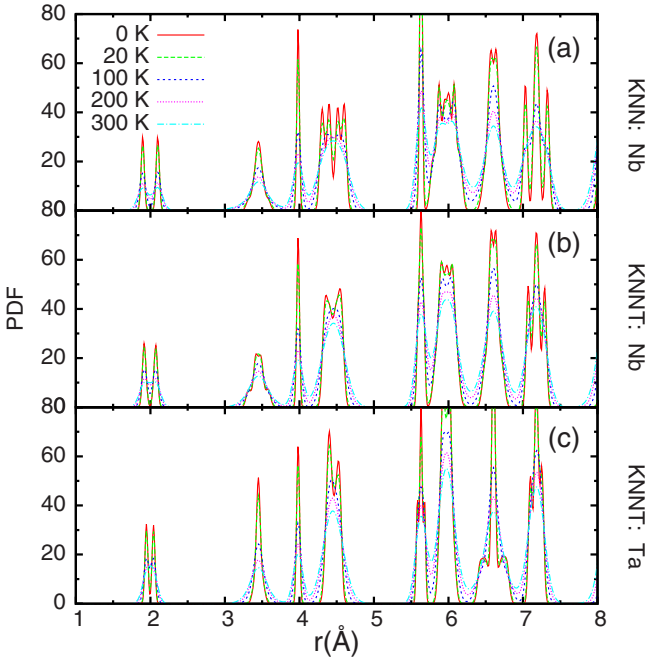

FIG. 2. (Color online) Harmonic PDF (arbitrary unit) of (a) Nb in KNN, (b) Nb in KNNT, and (c) Ta in KNNT at temperatures from 0 to 300 K and distance up to 8 Å.

≈3.93 Å, correspond to the *B*-site-*A*-site and *B*-site-*B*-site distances, respectively. In KNNT, the splitting of the first (*B*-site-O) peak for Nb is roughly 40% larger than that of Ta (0.25 Å vs 0.15 Å). However, the Nb first peak PDF splitting in KNN and KNNT are very similar. Thus from a structural point of view the off-centerings of both Nb and Ta are similar in KNN and KNNT and the main difference between these compounds is that Ta stays within ≈0.1 Å of the center of the TaO_6 octahedra. An interesting feature is that although all the peaks broaden with temperature, the third peak (*B*-site-*B*-site) remains sharper than the first or second peaks at high temperature. This means that the *B*-site motions remain correlated reflecting stiff force constants associated with the *B*-site-*B*-site distance. This is consistent with the calculations of Grinberg and co-workers on the low-temperature structures of related materials which they found could be understood using bond valence models.[45] Within this framework, displacement of a *B*-site ion toward an O drives the neighboring *B*-site bonded to the same O away from it. This type of interaction favors polar behavior.

We examine the temperature dependence of the PDF peak height located at $r \approx 1.92$ and 3.45 Å corresponding to the distance between O-*B*-site and *A*-site-*B*-site as shown in Fig. 3. Here the behavior agrees well between the two distances. The PDF peak height decreases as a function of temperature due to the broadening of PDF peak as a result of the thermal vibrations. The overall Ta PDF peak height is higher than those of Nb for every temperatures showing stiff force constant between Ta and Na/K atoms. In the lower temperature region, there is notable difference between the height of PDF peak of Nb in KNN and KNNT but the peaks become similar as the temperature reaches 50 K.

In the case of the *A*-site atoms (not shown), at low temperature, the lowest distance peak in the PDF for KNN and

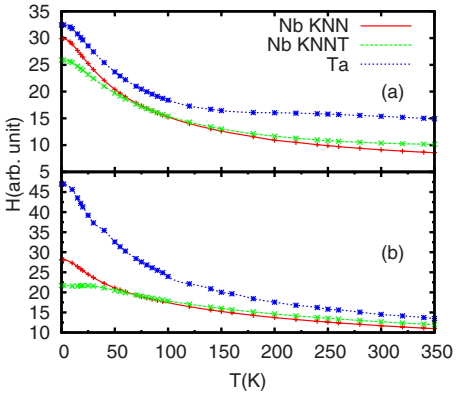

FIG. 3. (Color online) Height (H) of the PDF peaks for Nb and Ta in KNN and KNNT as a function of temperature (a) at the interatomic distance (r)=1.91 Å (for Nb cation in KNN), 1.92 Å (for Nb in KNNT), and 1.95 Å (for Ta in KNNT) and (b) at the interatomic distance (r)=3.45 Å (for Nb cation in KNN), 3.46 Å (for Nb cation in KNNT) and 3.45 Å (for Ta). In other words, peaks in (a) are the first peaks of PDFs in Fig. 2 representing the distance between O and Nb/Ta cations while peaks in (b) are the second peaks representing the distance between Na/K and Nb/Ta cations. The lines are there to guide the eyes.

KNNT is sharp and has a single maximum, while the corresponding Na PDF shows structure. This peak corresponds to the distance form the A site to the O in its 12-fold cage. The Na nearest-neighbor PDF peak is split into three subpeaks, such that the difference between the shortest and longest Na-O bond length is approximately 0.4 Å. The structure reflects the fact that the Na is off-centered while the K stays near the center of its cage. This Na off-centering reflects the smaller ionic radius of Na relative to K. It should also be noted that the behaviors of the A-site PDF in KNN and KNNT are very similar, indicating that the substitution on Ta has little effect on the A-site dynamics. Similarly, concentrating on the first PDF peak corresponding to the O cage of the Na, the splitting of KNN and KNNT are very similar, showing similar off-centering of Na. However, at low temperature the structure of the second peak (corresponding to the Na-B-site distance (in the ideal cubic perovsktie, 3.45 Å), is noticeably different between KNN and KNNT at low temperature, which reflects a difference in the structure of Ta off-centering as compared to Nb, as discussed above.

The mean-square displacements (MSDs) are given by

$$\langle u^2 \rangle = \frac{1}{M_\kappa} \sum_{j\mathbf{q}} \frac{E_j(\mathbf{q})}{\omega_j^2(\mathbf{q})} e(\kappa|j\mathbf{q}) e^*(\kappa|j\mathbf{q}), \tag{5}$$

where M_κ is the mass of atom κ, $E_j(\mathbf{q})$ is the mode energy, $\omega_j(\mathbf{q})$ is the frequency of dynamical matrix, and and $e(\kappa|j\mathbf{q})$ is the principle directions obtained from the eigenvectors of the dynamical matrix. Note that the temperature dependence is contained in $E_j(\mathbf{q})$ and that in the high-temperature classical limit the harmonic MSD is linear in temperature and depends on force constants but not masses while at low temperature, the MSD is proportional to $1/\sqrt{m}$. The MSD for the B-site atoms is shown in Fig. 4. As may be seen, KNNT is stiffer than KNN from the point of view of all atoms. However, the main difference is that the Ta MSD in KNNT is lower by ≈20% compared with Nb. The Nb MSD differs significantly from those of KNN and KNNT. While the PDF peak height between KNN and KNNT A-site-B-site atomic pairs is similar at $r \approx 1.92$ Å and 3.45 Å, the MSD shows that the overall behavior of Nb is less off-centered when adding Ta. This means that in addition to its tendency to stay near the center of its O cage, the Ta force constants are stiffer than those of Nb.

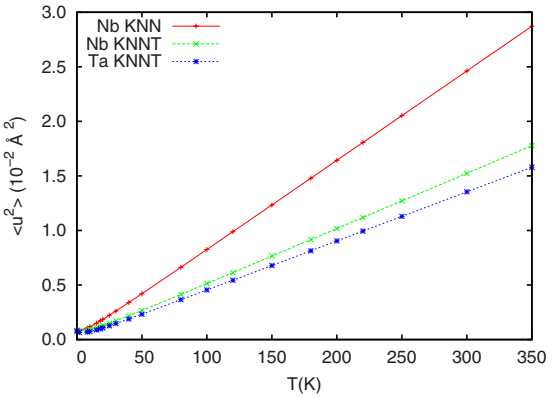

FIG. 4. (Color online) Mean-square displacement $\langle u^2 \rangle$ of B-site cations in KNN and KNNT. The lines are there to guide the eyes.

The harmonic temperature evolution of PDF for Nb atoms in the overall and dynamics of 10–20 meV range of frequency are depicted in Fig. 5. This frequency range is dominated by B-site cation motion. As may be seen, the peak at the B-site to B-site distance of 3.98 Å stays very sharp while

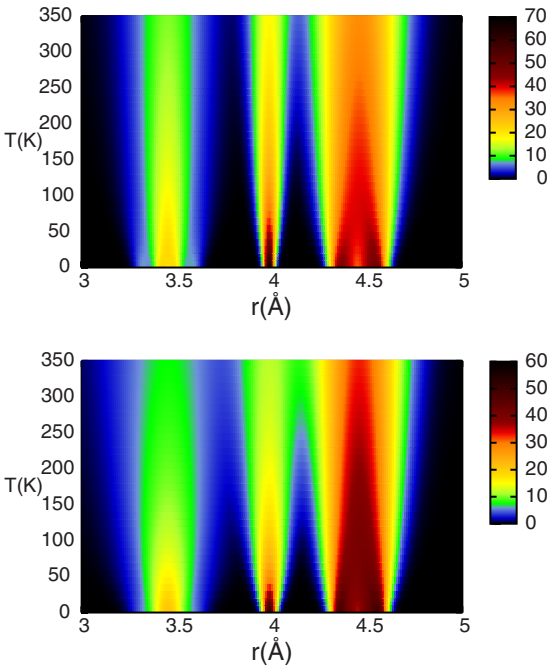

FIG. 5. (Color online) Temperature-dependent dynamical pair distribution function for Nb in KNNT including all frequency spectrums (upper panel) frequency ranges between 10 and 20 meV (lower panel). Color gradients refer to the height of the PDF peaks (in arbitrary units).

the other features broaden with temperature. This again shows that the stiffness of the *B*-site-*B*-site interaction leads to correlation of the *B*-site motions.

IV. SUMMARY AND CONCLUSIONS

In conclusions, we have investigated the local structure and harmonic level dynamics of pure and Ta-substituted $(K,Na)NbO_3$ using supercell calculations. We find that the structural effect of Ta is very short ranged consisting of a suppression of the off-centering on the Ta site, with some impact on the neighboring Nb. Similarly, the dynamics of the Nb *B*-site ions is suppressed by Ta addition, and the Ta shows stiffer force constants even though it is closer to the center of its O cage. This connects the lower T_C and resulting higher dielectric constant of the Ta-substituted material with a very local tendency for the Ta to off-center more weakly than Nb in this material.

ACKNOWLEDGMENTS

We are grateful for helpful discussions with T. Egami, M. Fornari, R. Kagimura, and W. Singhsomroje. This work was supported by the Department of Energy, Division of Materials Science and Engineering (D.J.S.) and the Office of Naval Research (M.S., D.J.S.), Mahidol University (M.S.).

[1] Y. Saito, H. Takao, T. Tani, T. Nonoyama, K. Takatory, T. Homma, T. Nagaya, and M. Nakamura, Nature (London) **432**, 84 (2004).
[2] J. Attia, L. Bellaiche, P. Gemeiner, B. Dkhil, and B. Malic, J. Phys. IV **128**, 55 (2005).
[3] Y. Guo, K. Kakimoto, and H. Ohsato, Appl. Phys. Lett. **85**, 4121 (2004).
[4] E. Hollenstein, M. Davis, D. Damjanovic, and N. Setter, Appl. Phys. Lett. **87**, 182905 (2005).
[5] Y. Kizaki, Y. Noguchi, and M. Miyayama, Appl. Phys. Lett. **89**, 142910 (2006).
[6] M. Kosec, V. Bobnar, M. Hrovat, J. Bernard, B. Malic, and J. Holc, J. Mater. Res. **19**, 1849 (2004).
[7] J. G. Fisher, A. Bencan, J. Holc, M. Kosec, S. Vernay, and D. Rytz, J. Cryst. Growth **303**, 487 (2007).
[8] E. Ringgaard and T. Wurlitzer, J. Eur. Ceram. Soc. **25**, 2701 (2005).
[9] K. Singh, V. Lingwala, S. C. Bhatta, N. S. Panwarb, and B. S. Semwa, Mater. Res. Bull. **36**, 2365 (2001).
[10] K. Wang and J. Li, Appl. Phys. Lett. **91**, 262902 (2007).
[11] H. Uršič, A. Benčan, M. Škarabot, M. Godec, and M. Kosec, J. Appl. Phys. **107**, 033705 (2010).
[12] I. Grinberg and A. M. Rappe, Appl. Phys. Lett. **85**, 1760 (2004).
[13] D. Fu, M. Endo, H. Taniguchi, T. Taniyama, and M. Itoh, Appl. Phys. Lett. **90**, 252907 (2007).
[14] M. Ahtee and A. W. Hewat, Acta Crystallogr., Sect. A: Cryst. Phys., Diffr., Theor. Gen. Crystallogr. **34**, 309 (1978).
[15] D. W. Baker, P. A. Thomas, N. Zhang, and A. M. Glazer, Appl. Phys. Lett. **95**, 091903 (2009).
[16] Y.-J. Dai, X.-W. Zhang, and K.-P. Chen, Appl. Phys. Lett. **94**, 042905 (2009).
[17] S. Zhang, R. Xia, and T. Shrout, J. Electroceram. **19**, 251 (2007).
[18] R.-P. Herber, G. A. Schneider, S. Wagner, and M. J. Hoffman, Appl. Phys. Lett. **90**, 252905 (2007).
[19] Y. Guo, K. Kakimoto, and H. Ohsato, Mater. Lett. **59**, 241 (2005).
[20] G. Zang, J. Wang, H. Chen, W. Su, C. Wang, P. Qi, B. Ming, J. Du, L. Zheng, S. Zhang, and T. R. Shrout, Appl. Phys. Lett. **88**, 212908 (2006).
[21] M. Matsubara, K. Kikuta, and S. Hirano, J. Appl. Phys. **97**, 114105 (2005).
[22] I. P. Raevskii, M. P. Ivliev, L. A. Reznichenko, M. N. Palatnikov, L. E. Balyunis, and M. A. Malitskaya, Tech. Phys. **47**, 772 (2002).
[23] S. Chu, W. Water, Y. Juang, and J. Liaw, Ferroelectrics **287**, 23 (2003).
[24] L. A. Reznichenko, O. N. Razumovskaya, L. A. Shikina, S. I. Dudkina, and A. V. Borodin, Tech. Phys. Lett. **28**, 83 (2002).
[25] L. Wu, J. Zhang, P. Zheng, and C. Wang, J. Phys. D **40**, 3527 (2007).
[26] Y. Zhou, M. Guo, C. Zhang, and M. Zhang, Ceram. Int. **35**, 3253 (2009).
[27] E. K. Akdoğan, K. Kerman, M. Abazari, and A. Safari, Appl. Phys. Lett. **92**, 112908 (2008).
[28] S. Zhang, R. Xia, H. Hao, H. Liu, and T. Shrout, Appl. Phys. Lett. **92**, 152904 (2008).
[29] K. Wang, J. Li, and N. Liu, Appl. Phys. Lett. **93**, 092904 (2008).
[30] D. Bilc and D. J. Singh, Phys. Rev. Lett. **96**, 147602 (2006).
[31] M. Matsubara, T. Yamaguchi, W. Sakamoto, K. Kituta, T. Yoko, and S. Hirano, J. Am. Ceram. Soc. **88**, 1190 (2005).
[32] R. D. Shannon, Acta Crystallogr., Sect. A: Cryst. Phys., Diffr., Theor. Gen. Crystallogr. **32**, 751 (1976).
[33] R. E. Cohen, Nature (London) **358**, 136 (1992).
[34] D. J. Singh, Phys. Rev. B **53**, 176 (1996).
[35] I.-K. Jeong, T. W. Darling, J. K. Lee, T. Proffen, R. H. Heffner, J. S. Park, K. S. Hong, W. Dmowski, and T. Egami, Phys. Rev. Lett. **94**, 147602 (2005).
[36] T. Egami, Z. Kristallogr. **219**, 122 (2004).
[37] T. Egami, Annu. Rev. Mater. Res. **37**, 297 (2007).
[38] *Planewaves, Pseudopotentials and the LAPW Method*, edited by D. J. Singh and L. Nordstrom (Kluwer Academic, Boston, 1994).
[39] D. J. Singh, Phys. Rev. B **43**, 6388 (1991).
[40] Local-orbital extensions to the LAPW basis were Na: *s*, *p*; K: *s*, *p*; Nb: *s*, *p*, *d*; Ta: *s*, *p*, *d*; O: *s*, *p*. The semicore states included in the valence were Na 2*s*, Na 2*p*, K 3*s*, K 3*p*, Nb 4*s*, Nb 4*p*, Ta 5*s*, and Ta 5*p*.
[41] *Thermal Vibrations in Crystallography*, edited by B. T. M. Willis and A. W. Pryor (Cambridge University Press, London, 1975).
[42] *Theory of Lattice Dynamics in the Harmonic Approximation*, edited by A. A. Maradudin, E. W. Montroll, G. H. Weiss, and I. P. Ipatova (Academic Press, New York, 1971).
[43] J. S. Chung and M. F. Thorpe, Phys. Rev. B **55**, 1545 (1997).
[44] J. S. Chung and M. F. Thorpe, Phys. Rev. B **59**, 4807 (1999).
[45] I. Grinberg and A. M. Rappe, Phase Transitions **80**, 351 (2007).